ACOUSTIC TOMOGRAPHY OF SOLAR CONVECTIVE FLOWS AND STRUCTURES

A.G. KOSOVICHEV
W.W. Hansen Experimental Physics Laboratory
Stanford University, CA 94305-4085

AND

T.L. DUVALL, JR.
Laboratory for Astronomy and Solar Physics
NASA Goddard Space Flight Center, Greenbelt, MD 20771

Abstract. We present a new method for helioseismic diagnostics of the three-dimensional structure of sound speed, magnetic fields and flow velocities in the convection zone by inversion of acoustic travel-time data. The data are measurements of the time for acoustic waves to travel between points on the solar surface and surrounding annuli obtained from continuous observations at the South Pole in 1991 and from high-resolution observations from the Solar and Heliospheric Observatory (SOHO) in 1996. The travel time of the waves depends primarily on the sound speed perturbations and the velocity of flow along the ray paths. The effects of the sound speed perturbations and flows can be separated by measuring the travel time of waves propagating in opposite directions along the same ray paths. Magnetic fields result in anisotropy of the wave speed. A 3D inversion method based on Fermat's Principle and a regularized least-squares technique have been applied to infer the properties of convection in the quiet Sun and in active regions.

Key words: solar physics, convection, time-distance helioseismology

1. Introduction

Observation of solar acoustic waves provides important information about the internal structure and dynamics of the Sun. The solar waves are ob-

served as 5-min oscillations of Doppler velocity or spectral-line intensity at the surface. The observations are usually represented in terms of normal modes of the Sun. Most research in helioseismology is focused on determining the internal stratification and rotation by inverting frequencies of the modes (Gough & Toomre, 1991). This traditional approach has provided interesting information about the radial structure, large-scale asphericity and differential rotation. However, using mode frequencies alone one could possibly study only azimuthally averaged, symmetrical relative to the equator components of the structure and rotation, whereas direct observations of the solar surface show substantial deviations from this symmetry. Therefore, considerable efforts in helioseismology are devoted to local helioseismic diagnostics, such as the ring-diagram analysis based on measuring the local dispersion relation of the acoustic waves (Gough & Toomre, 1983; Hill, 1988; Haber, *et al*, 1994; Bogdan & Braun, 1995), and the time-distance seismology based on travel times of groups of modes (Duvall, *et al.*, 1993, 1996; D'Silva & Duvall, 1995; Kosovichev, 1996).

In Section 2, we discuss some principles of time-distance helioseismology, interpretation of the travel time measurements in the acoustical ray approximation and the role of wave effects. Our numerical inversion procedure and test results are described in Section 3. In Section 4, we present some first inferences about convection in the quiet Sun and in active regions.

2. Time-distance seismology

2.1. OBSERVATION OF THE CROSS-COVARIANCE FUNCTION

The basic idea of time-distance helioseismology is to measure the acoustic travel time between different points on the solar surface, and then to use the measurement for inferring variations of the structure and flow velocities in the interior along the wave paths connecting the surface points. This idea is similar to the Earth's seismology. However, unlike in Earth, the solar waves are generated stochastically by numerous acoustic sources in the subsurface layer of turbulent convection. Therefore, to measure the wave travel time, we use the cross-covariance function, $\Psi(\tau, \Delta)$, of the oscillation signal, $f(t, \boldsymbol{r})$, between different points on the solar surface (Duvall, *et al.*, 1993):

$$\Psi(\tau, \Delta) = \int_0^T f(t, \boldsymbol{r}_1) f^*(t + \tau, \boldsymbol{r}_2) dt, \qquad (1)$$

where Δ is the angular distance between the points with coordinates $\boldsymbol{r}_1$ and $\boldsymbol{r}_2$, τ is the delay time, and T is the total time of the observations. Because of the stochastic nature of excitation of the oscillations, function Ψ must be averaged over some areas on the solar surface to achieve a signal-to-noise ratio sufficient for measuring travel times τ. The oscillation

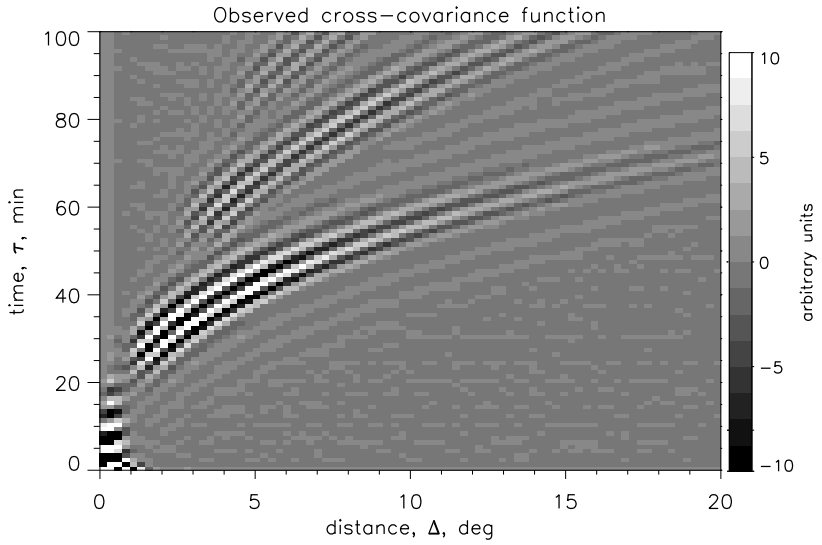

Figure 1. The observed cross-covariance function inferred from the data obtained at the South Pole by Jefferies *et al.* (1994) as a function of distance on the solar surface, Δ, and the delay time, τ.

signal, $f(t, \boldsymbol{r})$, is usually the Doppler velocity or intensity. A typical cross-covariance function averaged over the whole disk is shown in Figure 1. The observational data were obtained at the South Pole on January 5, 1991, by Jefferies *et al.* (1994). The oscillation signal was intensity variations of $Ca^{+}K$ line, filtered to select the p-mode frequency range using Gaussian transfer function

$$G(\omega) = \exp\left[-\left(\frac{\omega - \omega_0}{\delta\omega}\right)^2\right], \tag{2}$$

where ω is the cyclic frequency, ω_0 is the central frequency and $\delta\omega$ is the characteristic bandwidth of the filter. The cross-covariance function in Fig. 1 displays three sets of ridges which correspond to the first, second and third bounces of packets of acoustic wave packets from the surface.

The cross-covariance function represents a solar 'seismogram'. Ideally, the seismogram should be inverted to infer the structure and flows using a wave theory. However, in practice, like in terrestrial seismology (e.g. Aki & Richards, 1980) and oceanography (Munk, *et al.*, 1995), we have to use a different approximation, the most simple and powerful of which is currently the geometrical acoustic (ray) approximation. In the next Section, we discuss relations between the modal wave approach and the ray theory.

2.2. CROSS-COVARIANCE FUNCTION AND TRAVEL TIMES

Generally, the observed solar oscillation signal corresponds to radial displacement or pressure perturbation, and can be represented in terms of normal modes, or standing waves (e.g. Unno *et al.*, 1989):

$$f(t,r,\theta,\phi) = \sum_{nlm} a_{nlm}\xi_{nlm}(r,\theta,\phi)\exp(i\omega_{nlm}t + i\phi_{nlm}), \tag{3}$$

where n, l and m are the radial order, angular degree and angular order of a normal mode respectively, $\xi_{nlm}(r,\theta,\phi)$ is a mode eigenfunction in the spherical coordinates, r, θ and ϕ, ω_{nlm} is the eigenfrequency, and ϕ_{nlm} is an initial phase of the mode. Using equation (2), we express the cross-covariance function in terms of normal modes, and then represent it as a superposition of traveling wave packets. Such a representation is important for interpretation of the time-distance data, and for studying from the data the regional structures in the Sun. The correspondence between the normal modes and the wave packets has been discussed for surface oscillations in Earth's seismology (e.g. Ben-Menahem, 1964) and also for ocean waves (e.g. Tindle & Guthrie, 1974).

To simplify the analysis, we consider the spherically symmetrical case. For a radially stratified sphere, the eigenfunctions can be represented interms of spherical harmonics $Y_{lm}(\theta,\phi)$:

$$\xi_{nlm}(r,\theta,\phi) = \xi_{nl}(r)Y_{lm}(\theta,\phi), \tag{4}$$

where $\xi_{nl}(r)$ is the radial eigenfunction (e.g. Unno, *et al.*, 1989).

Then, from the convolution theorem (e.g. Bracewell, 1986):

$$\Psi(\tau,\Delta) = \int_{-\infty}^{\infty} F(\omega,\boldsymbol{r}_1)F^*(\omega,\boldsymbol{r}_2)\exp(i\omega\tau)d\omega, \tag{5}$$

where $F(\omega,\boldsymbol{r})$ is Fourier transform of the oscillation signal $f(t,\boldsymbol{r})$, filtered with the Gaussian transfer function (2). The time series used in our analysis are considerably longer than the travel time τ, therefore, we can neglect the effect of the window function, and represent $F(\omega,\boldsymbol{r})$ in the form

$$F(\omega,r,\theta,\phi) \approx \sum_{nlm} a_{nl}\xi_{nl}(r)Y_{lm}(\theta,\phi)\delta(\omega-\omega_{nl})\exp\left[-\left(\frac{\omega-\omega_0}{\delta\omega}\right)^2\right], \tag{6}$$

where $\delta(x)$ is the delta-function, and ω_{nl} are frequencies of the normal modes. In addition, we assume the normalization conditions: $\xi_{nl}(R) = 1$, $a_{nl} = 1$. Then, the cross-covariance function is

$$\Psi(\tau,\boldsymbol{r}_1,\boldsymbol{r}_2) = \sum_{nl}\sigma_{nl}\exp\left[-\left(\frac{\omega-\omega_0}{\delta\omega}\right)^2 + i\omega_{nl}\tau\right]\sum_{m=-l}^{l} Y_{lm}(\theta_1,\phi_1)Y^*_{lm}(\theta_2,\phi_2). \tag{7}$$

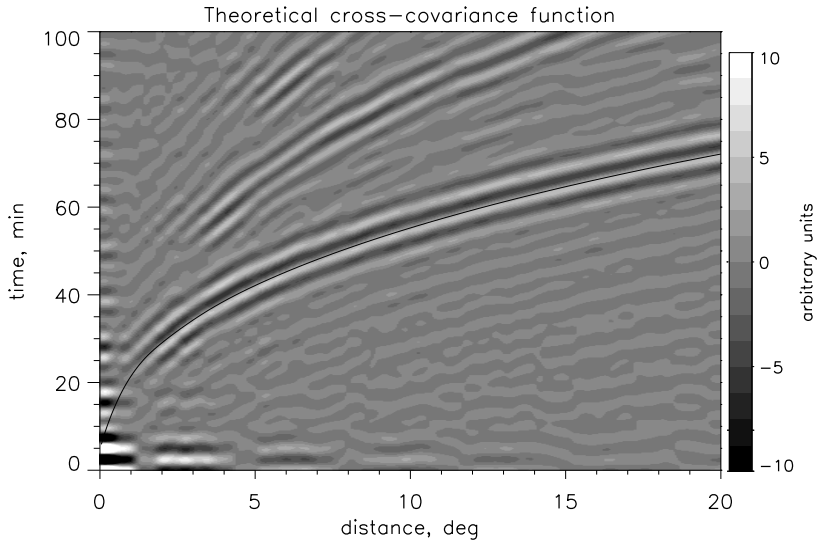

Figure 2. The theoretical cross-covariance function of the solar p-modes of $l = 0 - 1000$ as a function of distance on the solar surface, Δ, and time, τ.

The sum of the spherical function products

$$\sum_{m=-l}^{l} Y_{lm}(\theta_1, \phi_1) Y^*_{lm}(\theta_2, \phi_2) = \alpha_l P_l(\cos\Delta), \tag{8}$$

where $P_l(\cos\Delta)$ is the Legendre polynomial, Δ is the angular distance between points 1 and 2 along the great circle on the sphere, $\cos\Delta = \cos\theta_1\cos\theta_2 + \sin\theta_1\sin\theta_2\cos(\phi_2 - \phi_1)$, and $\alpha_l = \sqrt{4\pi/(2l+1)}$. Then, the cross-covariance function in terms of the normal modes

$$\Psi(\tau, \Delta) \approx \sum_{nl} a_{nl}\alpha_l P_l(\cos\Delta) \exp\left[-\left(\frac{\omega_{nl} - \omega_0}{\delta\omega}\right)^2 + i\omega_{nl}\tau\right]. \tag{9}$$

We use Eq.(9) to generate the cross-covariance function for solar models. An example of the theoretical cross-covariance function of p modes of the standard solar model of Christensen-Dalsgaard, *et al.* (1996) is shown in Fig. 2.

By grouping the modes in Eq. (9) in narrow ranges of the angular phase velocity, $v = \omega_{nl}/L$, where $L = \sqrt{l(l+1)}$, and applying the method of stationary phase, the cross-covariance function can be approximately represented in the form

$$\Psi(\tau, \Delta) \propto \sum_{\delta v} \cos\left[\omega_0\left(\tau - \frac{\Delta}{v}\right)\right] \exp\left[-\delta\omega^2\left(\tau - \frac{\Delta}{u}\right)^2\right], \tag{10}$$

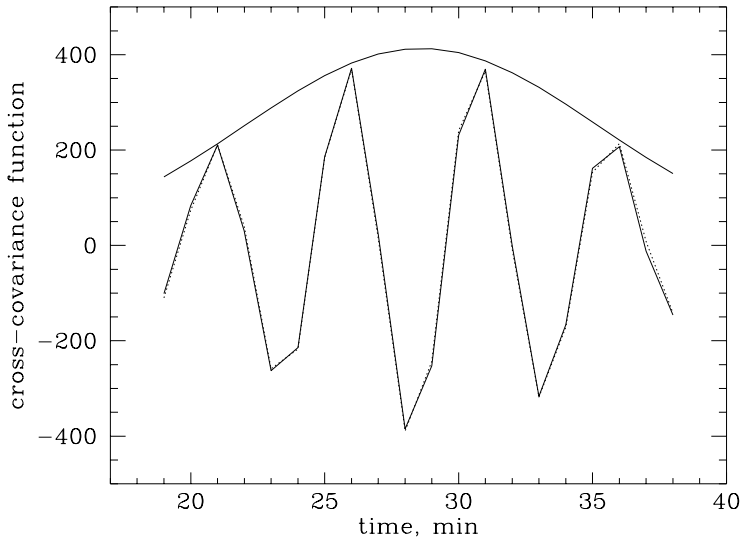

Figure 3. An example of the Gabor wavelet (Eq. 10) fit to a cross-covariance function obtained from the MDI data. The solid curves show the periodic component and the envelope of the wavelet; the dashed curved is the measured cross-covariance function.

where δv is a narrow interval of the phase speed, $u \equiv (\partial\omega/\partial k_h)$ is the horizontal component of the group velocity, $k_h = 1/L$ is the angular component of the wave vector, and ω_0 is the central frequency of the frequency filter (2), and $\delta\omega$ is the characteristic width of the filter. We measure the phase and group travel times by fitting individual terms of Eq. (10), represented by a Gabor-type wavelet, to the observed cross-covariance function using a least-squares technique. An example of the fit is shown in Fig.3.

This technique measures both phase (Δ/v) and group (Δ/u) travel times of the p-mode wave packets. The previous time-distance measurements provided either the group time (Jefferies, *et al.*, 1994), or an unspecified combination of the group and phase times (Duvall, *et al.*, 1996). We have found that the noise level in the phase-time measurements is substantially lower than in the group-time measurements. Therefore, in this paper, we use the phase times. We also use the geometrical acoustic (ray) approximation to relate the measured phase times to the internal properties of the Sun. More precisely, we measure the variations of the local travel times at different points on the surface, relative to the travel times averaged over the observed area, and then infer variations of the internal structure and flow velocities from the travel time anomalies using a perturbation theory.

2.3. TRAVEL TIME PERTURBATION

In the ray approximation, the travel times are sensitive only to the perturbations along the ray paths given by

$$\frac{d\boldsymbol{r}}{dt} = \frac{\partial \omega}{\partial \boldsymbol{k}}, \qquad \frac{d\boldsymbol{k}}{dt} = \frac{\partial \omega}{\partial \boldsymbol{r}}, \tag{11}$$

where $\boldsymbol{r}$ is the radius-vector and $\boldsymbol{k}$ is the wave-vector. The variations of the travel time obey Fermat's Principle (e.g. Gough, 1993)

$$\delta\tau = \frac{1}{\omega}\int_{\Gamma} \delta\boldsymbol{k} d\boldsymbol{r}, \tag{12}$$

where $\delta\boldsymbol{k}$ is the perturbation of the wave vector due to the structural inhomogeneities and flows along the unperturbed ray path, Γ.

The dispersion relation for acoustic waves in the convection zone is

$$(\omega - \boldsymbol{k}\boldsymbol{U})^2 = \omega_c^2 + \boldsymbol{k}^2 c_f^2, \tag{13}$$

where $\boldsymbol{U}$ is the flow velocity, ω_c is the acoustic cut-off frequency, $c_f^2 = \frac{1}{2}\left(c^2 + c_A^2 + \sqrt{\left(c^2 + c_A^2\right)^2 - 4c^2(\boldsymbol{k}\boldsymbol{c_A})^2/k^2}\right)$ is the fast magnetoacoustic speed, $\boldsymbol{c_A} = \boldsymbol{B}/\sqrt{4\pi\rho}$ is the vector Alfvén velocity, $\boldsymbol{B}$ is the magnetic field strength, c is the adiabatic sound speed, and ρ is the plasma density. If we assume that, in the unperturbed state $\boldsymbol{U} = \boldsymbol{B} = 0$, then, to the first-order approximation

$$\delta\tau = -\int_{\Gamma}\left[\frac{(\boldsymbol{n}\boldsymbol{U})}{c^2} + \frac{\delta c}{c}S + \left(\frac{\delta\omega_c}{\omega_c}\right)\frac{\omega_c^2}{\omega^2 c^2 S} + \frac{1}{2}\left(\frac{c_A^2}{c^2} - \frac{(\boldsymbol{k}\boldsymbol{c_A})^2}{k^2 c^2}\right)\right] ds, \tag{14}$$

where $\boldsymbol{n}$ is a unit vector tangent to the ray, $S = k/\omega$ is the phase slowness. Then, we separate the effects of flows and structural perturbations by taking the difference and the mean of the reciprocal travel times:

$$\delta\tau_{\text{diff}} = -2\int_{\Gamma}\frac{(\boldsymbol{n}\boldsymbol{U})}{c^2} ds; \tag{15}$$

$$\delta\tau_{\text{mean}} = -\int_{\Gamma}\left[\frac{\delta c}{c}S + \left(\frac{\delta\omega_c}{\omega_c}\right)\frac{\omega_c^2}{\omega^2 c^2 S} + \frac{1}{2}\left(\frac{c_A^2}{c^2} - \frac{(\boldsymbol{k}\boldsymbol{c_A})^2}{k^2 c^2}\right)\right] ds. \tag{16}$$

Anisotropy of the last term of Eq. (16) allows us to separate, at least partly, the magnetic effects from the variations of the sound speed and the acoustic cut-off frequency. The acoustic cut-off frequency, ω_c may be perturbed by the surface magnetic fields and by the temperature and density inhomogeneities. The effect of the cut-off frequency variation depends strongly

on the wave frequency, and, therefore, it should result in frequency dependence in $\tau_{\rm mean}$. However, we have not detected yet a significant frequency dependence in the observed travel times.

Typically, we measure times for acoustic waves to travel between points on the solar surface and surrounding quadrants symmetrical relative to the North, South, East and West directions. In each quadrant, the travel times are averaged over narrow ranges of travel distance Δ. Then, the times for northward-directed waves are subtracted from the times for south-directed waves to yield the time, $\tau^{\rm NS}_{\rm diff}$, which predominantly measures north-south motions. Similarly, the time differences, $\tau^{\rm EW}_{\rm diff}$, between westward- and eastward directed waves yields a measure of east-ward motion. The time, $\tau^{\rm oi}_{\rm diff}$, between outward- and inward-directed waves, averaged over the full annuli, is mainly sensitive to vertical motion and the horizontal divergence. This approximate separation onto the flow components provides a qualitative picture of the motions on the scale larger than the size of the quadrants, and is useful for a preliminary analysis. However, in our numerical inversion of the data (Sec. 3), all three components of the flow velocity are properly taken into account. The averaging procedure described here is essential for reducing noise in the data.

In addition, a similar averaging procedure is applied for $\tau_{\rm mean}$ to measure the times corresponding to the isotropic and anisotropic components of the structural perturbations. While the anisotropy can be estimated from the quadrant-averaged data, to separate the magnetic field components, $\tau_{\rm mean}$ is averaged over octants. We have found that the anisotropic component in the quiet Sun is substantially weaker than the isotropic component, even around magnetic structures of the chromospheric network.

2.4. WAVE EFFECTS

Obviously, we are concerned about the accuracy of the ray approximation, particularly, for short travel distances and small-scale perturbations. Because a wave theory for the time-distance seismology of the 3-D convective structures has not been developed, the precise limits of the spatial resolution of the ray approximation are not determined. However, we have studied the the resolution with depth, which is one of the main concerns, in particular, for short travel distances when the wavelength becomes comparable with the characteristic scale. In this study, we have carried out a 'hare-and-hounds' test for spherically symmetrical perturbations of the sound speed. The test procedure was the following. One of us (AGK) computed the theoretical cross-covariance functions, as described in Sec. 2.2, for a standard solar model and for the same model with a localized sound-speed

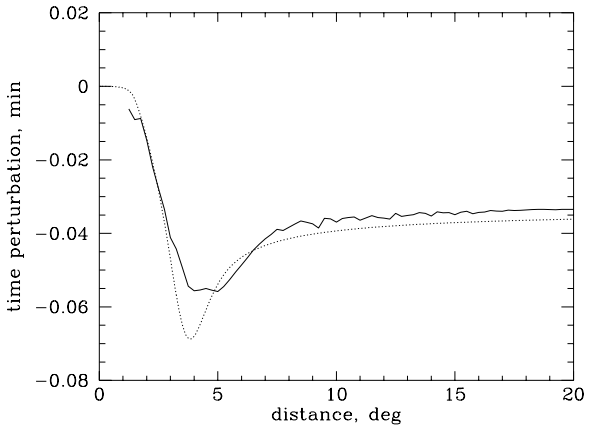

Figure 4. The travel time variation of the sound-speed perturbation (Eq. 17) with $A = 0.01, r_0 = 0.98R$, and $w = 0.005R$, estimated from the cross-covariance function (solid curve) and from the ray theory (dotted curve).

perturbation,

$$\delta c/c = A \exp[-0.5(r - r_0)^2/w^2], \tag{17}$$

where A is the amplitude of the perturbation, r_0 is the central radius, and w is the characteristic width of the perturbation.

$A = 0.01, r_0 = 0.98R$, and $w = 0.005R$. Then, the travel time difference between the cross-covariance functions of the two models were determined by the second author (TLD) without knowing the characteristics of the perturbation. The result of his measurements shown in Fig. 4 (solid curve) is in agreement with the travel time variation estimated from the ray theory. Evidently, the structure perturbations inferred in the ray approximation from the cross-covariance function will appear somewhat smoother than they are in reality.

Because of the wave effects, the travel time measured from the cross-covariance function depends not only on the perturbations along a ray path but on the perturbations in some vicinity of the ray path (cf Stark & Nikolayev, 1993; Bogdan, 1996). This is illustrated in Fig 5 which shows the energy density of a wave packet constructed using a normal-mode solution to the solar oscillation equations, and corresponding ray paths at three frequencies, 2.8, 3 and 3.5 mHz. The spreading along the ray path is partly taken into account in our analysis by averaging the travel times over a range of the travel distance. Beside the spreading, the wave packet also shows some patchy interference structure with depth, which is because the wave packet consists only of the modes of the radial order n of 1, 2 and 3.

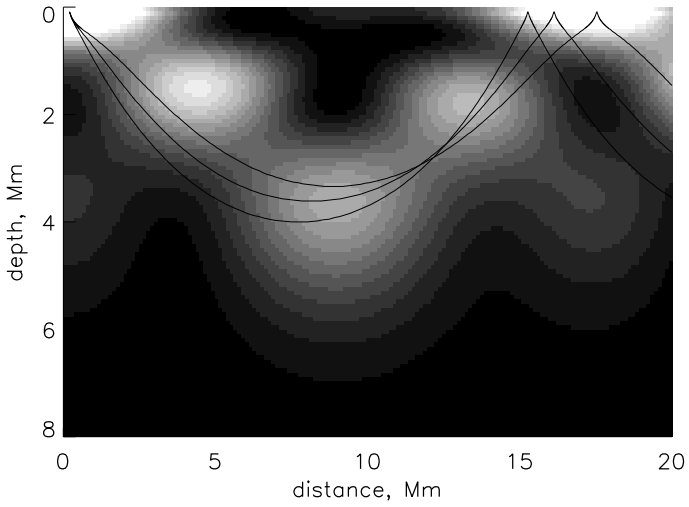

Figure 5. The energy density as a function of the depth and distance of a wave packet (gray-scale image), and the corresponding ray paths of the frequencies 2.8, 3, and 3.5 mHz.)

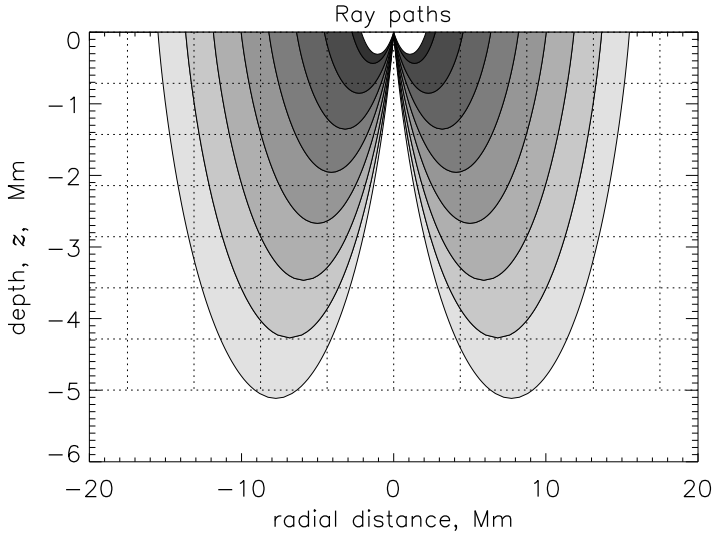

Figure 6. The regions of ray propagation (shaded areas) as a function of depth, z, and the radial distance, Δ, from a point on the surface. The rays are also averaged over a circular regions on the surface, forming three-dimensional figures of revolution. The dashed lines are the boundaries of the cells of the inversion model.

3. Inversion method

3.1. DISCRETE MODEL

We assume that the convective structures and flows do not change during the observations and represent them by a discrete model. In this model, the 3-D region of wave propagation is divided into rectangular blocks. The perturbations of the sound speed and the three components of the flow velocity are approximated by linear functions of coordinates within each block, e.g.

$$\boldsymbol{U}(x,y,z) = \sum \boldsymbol{C}_{ijk} \left[1 - \frac{|x - x_i|}{x_{i+1} - x_i}\right] \left[1 - \frac{|y - y_j|}{y_{j+1} - y_j}\right] \left[1 - \frac{|z - z_k|}{z_{k+1} - z_k}\right], \tag{18}$$

where x_i, y_j, z_k are the coordinates of the rectangular grid, $\boldsymbol{C}_{ijk}$ are the values of the velocity in the grid points, and $x_{i-1} \le x \le x_{i+1}$, $y_{j-1} \le y \le y_{j+1}$, and $z_{k-1} \le z \le z_{k+1}$. A part of the $x - z$ grid is shown in Fig.6 together with the ray system used in the inversions.

The travel time measured at a point on the solar surface is the result of the cumulative effects of the perturbations in each of the traversed rays of the 3D ray systems. Figure 6 shows, in the ray approximation, the sensitivity to given subsurface location for a certain point on the surface. This pattern is then moved around for different surface points in the observed area, so that overall the data are sensitive to all subsurface points in the depth range 0-5 Mm.

Therefore, we average the equations over the ray systems corresponding to the different radial distance intervals of the data, using approximately the same number of ray paths as in the observational procedure. As a result, we obtain two systems of linear equations that relate the data to the sound speed variation and to the flow velocity, e.g. for the velocity field,

$$\delta\tau_{\mathrm{diff};\lambda\mu\nu} = \sum_{ijk} \boldsymbol{A}^{ijk}_{\lambda\mu\nu} \cdot \boldsymbol{C}_{ijk}, \tag{19}$$

where vector-matrix $\boldsymbol{A}$ maps the structure properties into the observed travel time variations, and indexes λ and μ label the location of the central point of a ray system on the surface, and index ν labels surrounding annuli. These equations are solved by a regularized least-squares technique (Paige & Saunders, 1982).

3.2. RESOLUTION AND ACCURACY

To test the resolution and accuracy of the inversions we took a simple model of multi-level convective flow, and computed the averaged travel times for the ray system shown in Fig.6 in the ray approximation.

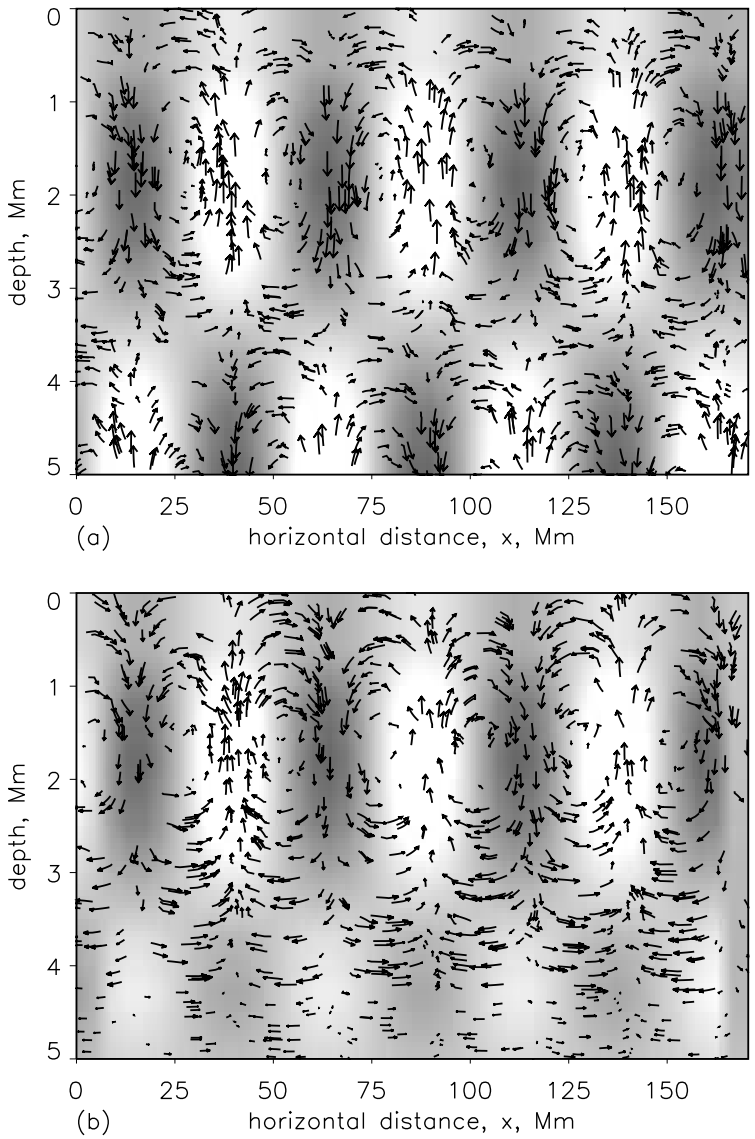

Figure 7. (a) A vertical cut of the flow pattern (arrows) and the sound-speed perturbation (grey-scale background) of the test model of convection; (b) the result of inversion of the travel times computed for the system of rays shown in Fig.6.

The results of inversion of the test data in comparison with the original model are shown in Figures 7 and 8. These results demonstrate a very accurate reconstruction of the horizontal components of the flow. However, the vertical flow in the deep layers is not resolved because of the predominantly

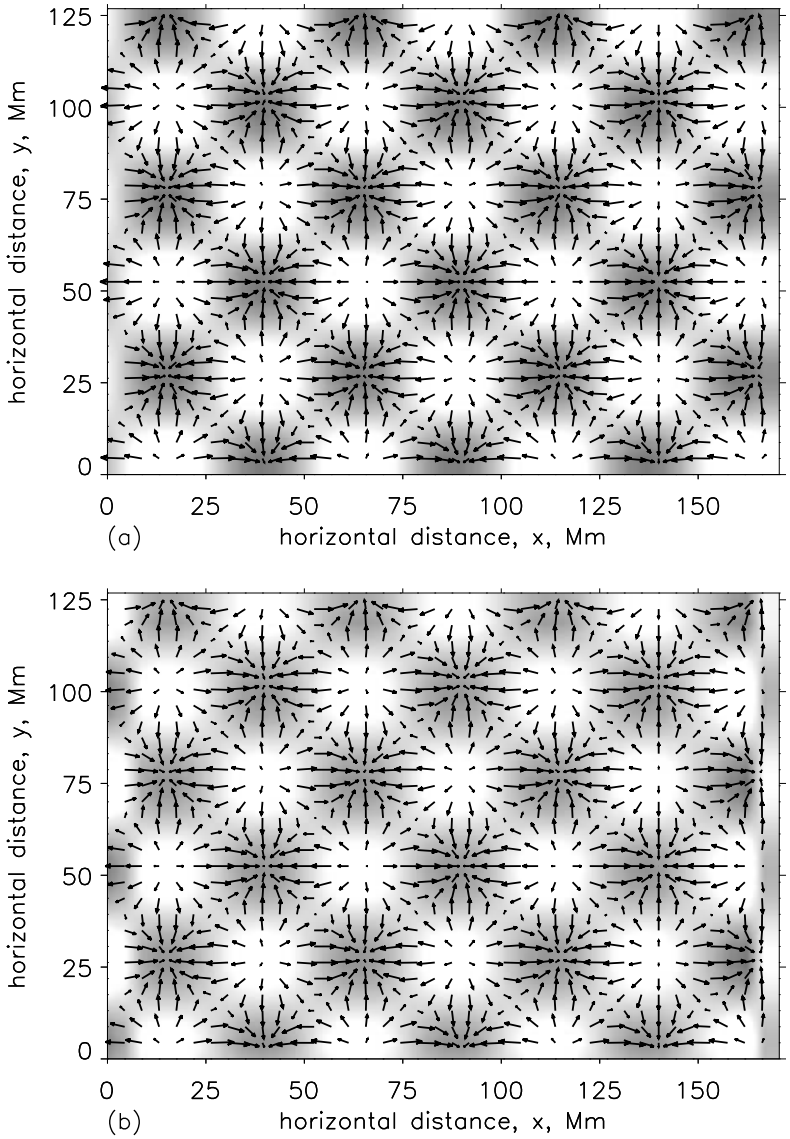

Figure 8. (a) The horizontal flows (arrows) and the sound-speed perturbation (grey-scale background) of the test model of convection at depth 4.2 Mm; (b) the result of inversion of the travel times computed for the system of rays shown in Fig.6.

horizontal propagation of the rays in these layers. The vertical velocities are also systematically underestimated by 10-20% in the upper layers.

4. Initial inversion results

4.1. QUIET-SUN CONVECTION

Using the techniques of time-distance helioseismology, we have investigated near-surface convective flows and structures using Doppler shift data from the SOI/MDI experiment on SOHO. The data used were for 8.5 hours on 27 January, 1996 from the high resolution mode of the MDI instrument. In this mode, the image sampling is 0.44 Mm per pixel, and the image quality is excellent, as compared with groundbased observations. This enables us to study the subsurface structure of convection seen at the surface. Signal-to-noise ratio is enhanced at the expense of spatial resolution by averaging the cross-covariance function in spatial blocks of $0.36^\circ \times 0.36^\circ$. The data are remapped onto a longitude, sine of latitude coordinate system. A solid body rotation at the Carringtion rate is removed by shifting the pictures in longitude. To isolate p-mode waves, the Gaussian filter (2) of full width at half-maximum 2 mHz and centered at 3.5mHz is applied to the temporal signal at each resultant point.

The travel time is determined by measuring displacements of the ridges of the cross-covariance function at different points on the solar surface, as described in Sec. 2. To examine waves at distances Δ shorter than 1 degree, a spatial-frequency filter was applied that multiplied the spatial Fourier transform by $k_h^{1.5}$, where k_h is the horizontal wave number.

The results of inversion of the data are shown in Figures 9 and 10. We have found that, in the upper layers, 2-3 Mm deep, the horizontal flow is organized in supergranular cells, with outflows from the center of the supergranules. The characteristic size of the cells is 20-30 Mm. Comparing with MDI magnetograms, we have found that the cells boundaries coincides with the areas of enhanced magnetic field. These results are consistent with the observations of supergranulation on the solar surface (e.g. Title, *et al.*, 1989). However, in the layers deeper than 2-3 Mm, we do not see the supergranulation pattern which suggests that supergranulation is a superficial phenomenon. The vertical flows (Fig. 10) correlate with the supergranular pattern in the upper layers. Typically, there are upflows in the 'hotter' areas where the sound speed is higher than average, and downflows in the 'colder' areas.

These initial results look very promising for studying supergranulation which certainly plays a very important role in the global dynamics of the Sun, but have not been understood. Our results question the original idea by Simon and Leighton (1964) that supergranulation represents large-scale convective cells driven by convective instability in the HeII ionization zone and, therefore, is, at least, 13 Mm deep. We hope to be able to observe the flow pattern at this depth and investigate how it develops with time.

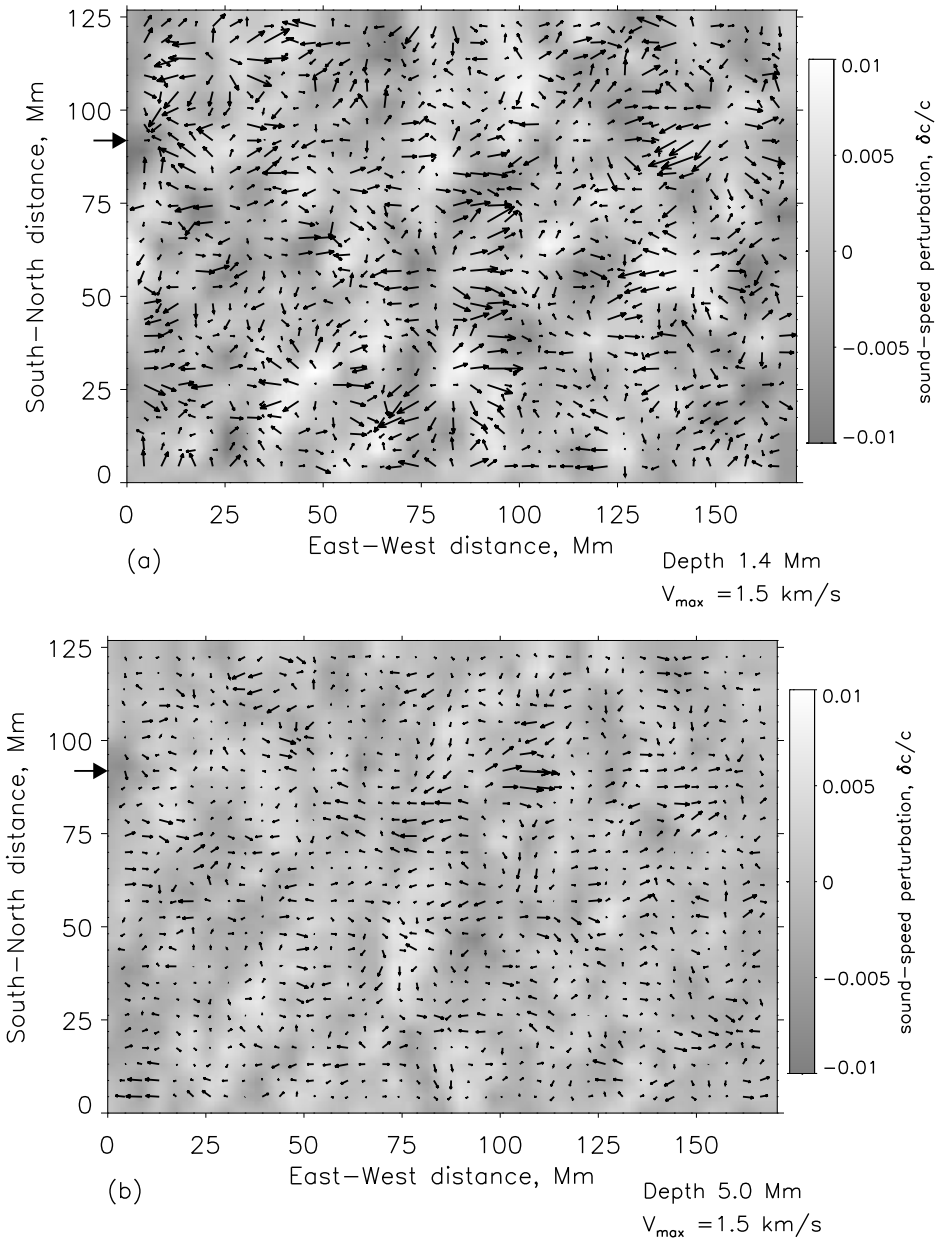

Figure 9. The horizontal flow velocity field (arrows) and the sound-speed perturbation (grey-scale background) at the depths of 1.4 Mm (Fig. 9a) and 5.0 Mm (Fig. 9b), as inferred from the SOHO/MDI high-resolution data of 27 January 1996. The arrows at the South-North axis indicate location of the vertical cut in East-West direction, which is shown in Fig. 10.

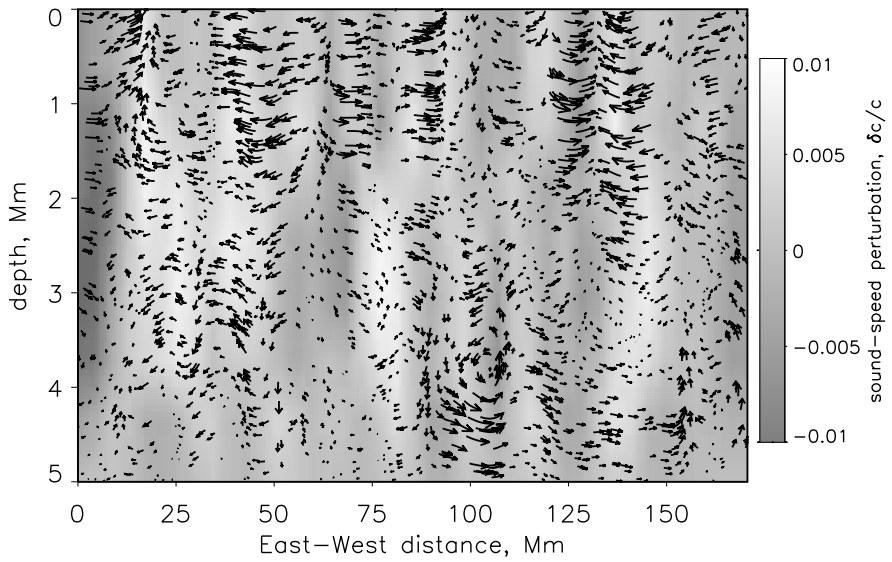

Figure 10. The vertical flow field (arrows) and the sound-speed perturbation (grey-scale background) at the North-South position indicated by arrows in Fig. 9.

4.2. LARGE-SCALE STRUCTURES AND FLOWS IN ACTIVE REGIONS

There is no high-resolution data available yet to study convection of the active Sun. However, we have studied some large-scale properties of convection using the data obtained at the South Pole by Jefferies *et al.* (1994) in January 1991, when the solar activity was high. The observed area is shown in the $Ca^{+}K$-line intensity map in Fig. 11a. The travel times in this area have been measured by Duvall *et al.* (1996) for four sets of rays propagating from each of 72×52 points equally spaced in the observed area to the surrounding annuli. The four radial distance ranges Δ were 2.5–4.25, 4.5–7, 7.25–10, and 10.25–15 heliographic degrees. Only $\tau^{\rm oi}_{\rm diff}$ and $\tau_{\rm mean}$ defined in Sec. 2.3 were used in this case.

For inversion of these data, we have adopted a four-layer discrete model described by Kosovichev (1996). The layers which all are 16 Mm thick have been divided into 72×52 rectangular blocks of approximately the same size as the spacing between the data points.

The inversion results have shown that perturbations of the active regions can be seen in the two upper layers, at 0-32 Mm, but not deeper. The three components of the flow velocity in the upper layer, inferred from the data, are illustrated in Fig. 11b. The results show strong downflows of ≈ 1 km/s around the sunspots, and some much weaker isolated upflows at

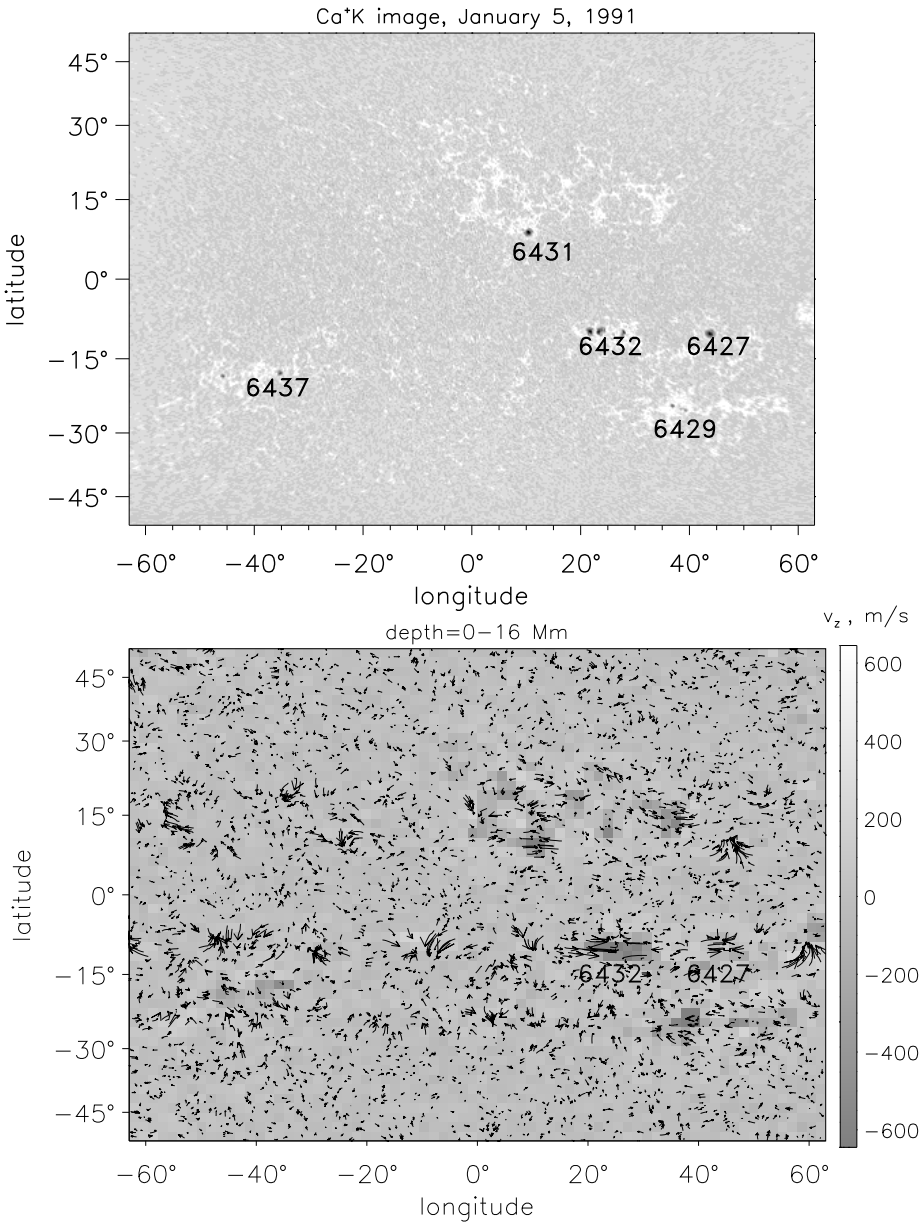

Figure 11. (a) $Ca^{+}K$-line image of the observed area observed by Jefferies *et al.* (1994) on 5 January 1991 at the geographical South Pole; (b) The horizontal (arrows) and vertical (grey-scale background) flow velocities in the subsurface layer of the area shown in Fig. 11a. (after Kosovichev, 1996)

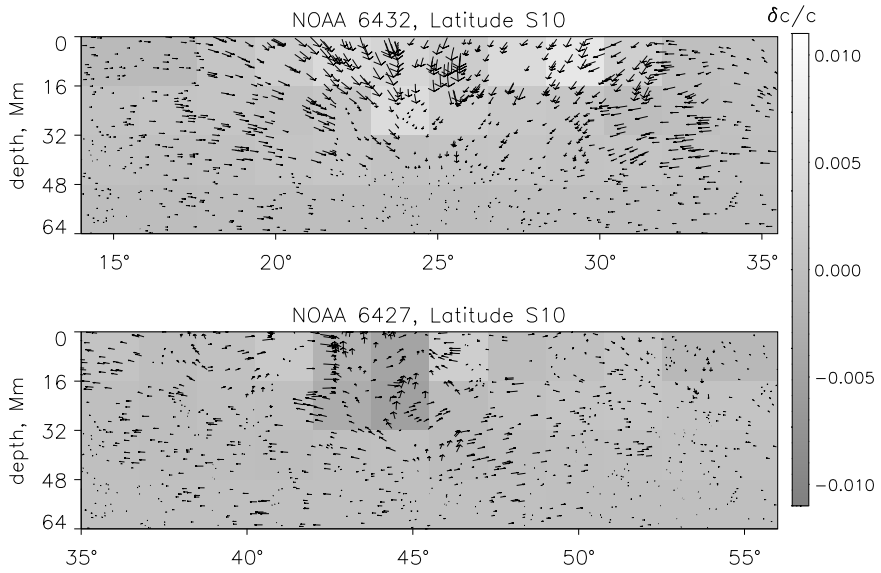

Figure 12. Variations of the sound speed (grey-scale map) and the flow velocity (arrows) as a function of depth and longitude at latitude $-10°$ in growing active region NOAA 6432 (top), and in decaying region NOAA 6427 (bottom). (Kosovichev, 1996)

the boundaries of the active latitudes. The spatial resolution of the data is insufficient to study the structure and dynamics of individual sunspots. However, it is interesting to note that the peak of the downdraft velocity is observed between the spots in the bipolar group NOAA 6432 located at latitude $-10°$ and longitude $20°$. This group results in two separate strong negative sound-speed perturbations in the top layer (0-16 Mm), which merge into a single perturbation in the second layer (16-32 Mm). Figure 12 (top) shows a vertical cut through this active region at a fixed latitude. The grey-scale map represents the sound speed structure, and the arrows - the projection of the velocity field into the longitude-depth plane. The convergent character of the flow is evident. This active region was only about 5 days old. The other young active regions in the observed area seem to show a similar pattern. Contrary, the much older decaying region NOAA 6427 (Fig.12, bottom) shows reduced sound speed and diverging upflow. Another active region, NOAA 6437, with similar characteristics disappeared a day after it was observed. It is also interesting to note that in the flow map (Fig. 11b), the largest flow velocities are observed at the active latitudes $\pm 10°$ and $\pm 22°$. Some areas show strong flows without any apparent activity. One could speculate, that at least, some of them could be the places where new magnetic structures emerged later; e.g. the area

of strong converging flow seen in the two upper layers at latitude -8° and longitude 10° was close to the place where a new large group of sunspots, NOAA 6440, was born two days after.

5. Conclusion

Time-distance helioseismology provides unique information about 3-D structures and flows associated with magnetic field and turbulent convection. This technique is at the very beginning of its development. In this paper, we have presented some basic principles of the technique and some initial results of inversion of the travel-time data obtained from the MDI experiment onboard SOHO (Scherrer, *et al.*, 1995), and from the geographical South Pole (Jefferies, *et al.*, 1994). The initial results reveal the internal structure of supergranulation flows, indicating that the divergent outflow in supergranules is only 2–3 Mm deep. The time-distance results also reveal large-scale subsurface sound-speed structures and flows related to the active regions. Also, there is evidence of different flow patterns and sound-speed structures in the developing and decaying regions.

Obviously, continuous long-term high-resolution observations are necessary to study the dynamics of solar convection in the quiet and active regions in detail.

Acknowledgements. We are grateful to Danmarks Grundforskningsfonden and TAC for sponsoring the workshop. This research is partly supported by the SOI-MDI NASA contract NAG5-3077 at Stanford University.

References

Aki, K. & Richards, P., (1980) *Quantitative Seismology. Theory and Methods*, San Francisco: Freeman.

Ben-Menahem, A., (1964) *Bull. Seism. Soc. America*, **54**, 1315.

Bogdan, T.J., 1996, *Bull. Amer. Astr. Soc.*, **28**, 937.

Bogdan, T.J. and Braun, D.C., (1995) in: Fourth SOHO Workshop *Helioseismology.* Proceedings - Invited Reviews and Working Group Reports (ESA SP-376) Paris, France: ESA, p. 31.

Bracewell, R.N., (1986) *The Fourier Transform and Its Applications*, Second Ed., New York, McGraw-Hill.

Duvall, T.L., Jr.,, Jefferies, S.M., Harvey, J.W., and Pomerantz, M.A., (1993) *Nature*, **362**, 430

Duvall, T.L.Jr., D'Silva, S., Jefferies, S.M., Harvey, J.W. & Schou, J., (1996) *Nature*, **379**, 235.

Christensen-Dalsgaard, J., Thompson, M.J., (1993) *AA* **272**, L1

Gough, D.O., (1993) in: *Astrophysical Fluid Dynamics*, Eds. J.-P. Zahn and J. Zinn-Justin, Elsevier Science Publ., p. 339.

Gough, D.O., and Toomre, J., (1983) *Solar Phys.*, **82**, 401

Gough, D.O., and Toomre, J., (1991) *Ann. Rev, Astron. Astrophys.*, **29**, 627

Haber, D.A., Toomre, J., Hill, F., and Gough, D., (1994) in *GONG 1994: Seismic Investigation of the Sun and Stars.* Conference Proceedings, Los Angeles California, 16-20

May 1994. R. Ulrich, ed. (Astronomical Society of the Pacific)
Hill, F., (1988) *ApJ*, **333**, 996
Jefferies, S.M., Osaki, Y., Shibahashi, H., Duvall, T.L., Jr., Harvey, J.W., and Pomerantz, M.A., (1994) *ApJ*, **434**, 795.
Kosovichev, A.G., (1996) *ApJL*, **461**, L55
Munk, W., Worcester, P., and Wunsch, C., (1995) *Ocean Acoustic Tomography*, Cambridge University Press, Cambridge.
Paige, C.C. and Saunders, M.A., (1982) *ACM Trans. Math. Software*, **8**, 43.
Scherrer,P.H., Bogart, R.S., Bush, R.I., Hoeksema, J.T., Kosovichev, A.G., Schou, J., Rosenberg, W., Springer, L., Tarbell, T.D., Title, A., Wolfson, C.J., Zayer, I. and the MDI Engineering Team, (1996) *Solar Phys.*, **162**, 129.
D'Silva, S. and Duvall, T.L., Jr., (1995) *ApJ*, **438**, 454.
Simon, G.W., and Leighton, R.B., (1964), *ApJ*, **140**, 1120.
Stark, P.B., and Nikolayev, D.I., (1993) *J. Geophys. Res.*, **98**, 8095.
Tindle, C.T., and Guthrie, K.M., (1974) *J. Sound and Vibr.*, **34**, 291.
Title, A.M., Tarbell, T.D., Topka, K.P., Ferguson, S.H., and Shine, R.A., (1989) *ApJ*, **336**, 475.
Unno, W., Osaki, Y., Ando, H., Saio, H., Shibahashi, H., (1989) *Nonradial Oscillations of Stars*, University of Tokyo Press, Tokyo.